Influence of regional development policies and clean technology adoption on future air pollution exposure

Mark Hixson [a], Abdullah Mahmud [a], Jianlin Hu [b], Song Bai [a], Debbie A. Niemeier [a], Susan L. Handy [c], Shengyi Gao [c], Jay R. Lund [a], Dana Coe Sullivan [d], Michael J. Kleeman [a,*]

[a] Department of Civil and Environmental Engineering, University of California, Davis, 1 Shields Avenue, Davis, CA 95616, USA
[b] Atmospheric Science Graduate Group, University of California, Davis, 1 Shields Avenue, Davis, CA 95616, USA
[c] Department of Environmental Science and Policy, University of California, Davis, 1 Shields Avenue, Davis, CA 95616, USA
[d] Sonoma Technology Inc., Petaluma, CA 94954, USA

ARTICLE INFO

ABSTRACT

Future air pollution emissions in the year 2030 were estimated for the San Joaquin Valley (SJV) in central California using a combined system of land use, mobile, off-road, stationary, area, and biogenic emissions models. Four scenarios were developed that use different assumptions about the density of development and level of investment in transportation infrastructure to accommodate the expected doubling of the SJV population in the next 20 years. Scenario 1 reflects current land-use patterns and infrastructure while scenario 2 encouraged compact urban footprints including redevelopment of existing urban centers and investments in transit. Scenario 3 allowed sprawling development in the SJV with reduced population density in existing urban centers and construction of all planned freeways. Scenario 4 followed currently adopted land use and transportation plans for the SJV. The air quality resulting from these urban development scenarios was evaluated using meteorology from a winter stagnation event that occurred on December 15th, 2000 to January 7th 2001. Predicted base-case PM2.5 mass concentrations within the region exceeded 35 μg m^{-3} over the 22-day episode. Compact growth reduced the PM2.5 concentrations by ~1 μg m^{-3} relative to the base-case over most of the SJV with the exception of increases (~1 μg m^{-3}) in urban centers driven by increased concentrations of elemental carbon (EC) and organic carbon (OC). Low-density development increased the PM2.5 concentrations by 1–4 μg m^{-3} over most of the region, with decreases (0.5–2 μg m^{-3}) around urban areas. Population-weighted average PM2.5 concentrations were very similar for all development scenarios ranging between 16 and 17.4 μg m^{-3}. Exposure to primary PM components such as EC and OC increased 10–15% for high density development scenarios and decreased by 11–19% for low-density scenarios. Patterns for secondary PM components such as nitrate and ammonium ion were almost exactly reversed, with a 10% increase under low-density development and a 5% decrease under high density development. The increased human exposure to primary pollutants such as EC and OC could be predicted using a simplified analysis of population-weighted primary emissions. Regional planning agencies should develop thresholds of population-weighted primary emissions exposure to guide the development of growth plans. This metric will allow them to actively reduce the potential negative impacts of compact growth while preserving the benefits.

© 2009 Elsevier Ltd. All rights reserved.

1. Introduction

Numerous studies have found correlations between negative human health effects and the concentration of airborne particulate matter with aerodynamic diameter less than 2.5 μm (PM2.5) (see for example Englert, 2004). Many counties within the United States currently violate 24-h average PM2.5 National Ambient Air Quality Standards (NAAQS) (see SI Figure S1). Residents within these counties usually want to improve their air quality, but it is unclear how they can enact local policies to achieve this goal. The largest sources such as on-road motor vehicles and major point sources are regulated directly by the federal government with no additional controls possible at the local level. Population expansion is encouraged as an economic benefit but it puts upward pressure on pollution emissions. Shifts in societal values and lifestyles such as low-density housing developments and larger cars also put upward pressure on emissions.

* Corresponding author. Tel.: +1 530 752 8386; fax: +1 530 752 7872.
E-mail address: mjkleeman@ucdavis.edu (M.J. Kleeman).

Despite the challenges listed above, a variety of local policies have been proposed across the United States to improve air quality. These include investments in public transit, encouragement for energy efficiency, bans on residential wood combustion, bans on certain agricultural practices, and adoption of "smart growth" policies that encourage more compact urban development with higher densities and greater mixing of land uses while preserving open space and agricultural land. Although emissions reduction estimates based on policy by policy analysis exist for some of these strategies, frequently these emissions reductions are not translated into quantitative changes in air quality, nor are they considered as part of an integrated system.

The San Joaquin Valley (SJV) in central California represents an interesting case study for the effect of local policies on air quality. The SJV is the largest contiguous region in the United States violating both the 24-h average NAAQS and the annual average NAAQS for PM2.5 (see SI Figure S1). Maximum PM2.5 concentrations in the SJV are among the highest recorded anywhere in the country (Magliano et al., 1999; Herner et al., 2005). The SJV is expected to double in population from 3 M to 6 M over the next 25–50 years (State of California, Department of Finance, 1998) leading to rapid changes in transportation, industry, agriculture, and power generation with associated changes in air pollutant emissions. The SJV therefore represents an ideal location to study how local policy choices will impact the future of air quality at the urban and regional scale in the United States.

In the present study, four scenarios for future growth in the SJV are tested for the year 2030. Each scenario shares a common assumption about total population growth in the region but they differ on policies about population density, land-use controls, transportation infrastructure, and supplemental controls for air pollution emissions. The future air quality outcomes for each scenario are predicted using the meteorological patterns experienced during a previous air pollution episode. The results show how the best choice of the local policies summarized above will improve air pollution in this region, and by extension, how other regions might benefit from similar policies.

2. Background

Past studies have linked compact urban development with lower levels of vehicle travel and mobile emissions (Krizek, 2003; Handy, 2005). Sprawling development has been linked to higher mobile emissions and to increased energy usage (Brownstone and Golob, 2009). One of the more detailed assessments of compact growth has shown reductions in the vehicle miles traveled by up to 10% in a region when compared to a "business-as-usual" strategy for growth projected to the year 2050 (Stone et al., 2007). A future land-use scenario assessment for Southern California found air quality improvements for ozone from more compact urban centers and higher emissions from a sprawl scenario (Kahyaoglu-Koracin et al., 2009). This previous work has focused primarily on the relationship of land-use change to emissions without considering changes to technology adoption. One metric which has been lacking from these previous efforts is an analysis of population-weighted exposure to PM2.5 concentrations.

3. Methods

3.1. Base-case 2030 emissions

The base emissions data for the SJV was a spatially (4 km) and temporally (1 h) resolved emissions inventory for area, point, and non-road mobile sources for the year 2002 produced by the California Air Resources Board (CARB). Generic growth factors for future emissions in different area and point categories were obtained from the California Emission Forecasting System (CEFS). CEFS does not include growth factors for most non-road mobile sources and so these growth factors were obtained from a previous study that utilized CARB's OFFROAD model (Puri and Kleinhenz, 1994). CEFS/OFFROAD growth factors were improved for the sources in the SJV that are expected to dominate future emissions of reactive organic gases (ROG), oxides of nitrogen (NOx) and total suspended particulate matter (TSP). Local growth activity data within the SJV was collected for sources within the top 9 categories: oil production, natural gas production, petroleum refining, civilian aircraft, rail yards, cogeneration, wine fermentation, foam manufacturing, and the port of Stockton. Previous estimates from CEFS for these source categories were based on economic model outputs and other socio-economic data that did not necessarily reflect local conditions in the SJV. For example, CEFS foam manufacturing growth factors were based on modeled forecasts of output from the plastics manufacturing sector which indicated that foam manufacturing activity would more than double between 2000 and 2030. However, information gathered from industry representatives and individual facilities in the SJV indicated that demand for the type of foam products manufactured in the SJV was actually in decline. The original and revised annual growth factors for the updated sources are −0.9/−2.6% (oil production), 1.2/−2.5% (natural gas production), 0/0.5% (petroleum refining), 1.0/0.4% (civilian aircraft), 1.8/1.2% (rail yards), 1.9/0.6% (cogeneration), 0.4/2.1% (wine fermentation), 3.6/0.9% (foam manufacturing) and −1.1/11.8% (Port of Stockton). The Port of Stockton emissions include only commercial maritime vessels and port equipment. Some investigation was made into future trends in ground-based cargo movement (rail vs. truck), but no firm data could be identified to replace existing growth forecasts. Future growth factors for emissions in all area, point, and non-road mobile categories were scaled down to reflect current control measures planned by CARB.

Future emissions from mobile sources in California in counties outside the SJV were scaled up from a CARB 2000 mobile emissions inventory using the growth factors contained in CEFS. Mobile emissions within the SJV were calculated using a modeling system composed of a GIS-based land-use model (UPlan), a four-step travel demand model (specified in TP+/Viper), and a new mobile emissions inventory model (UCDrive-MOBILE). UPlan is a rule-based urban growth model that allocates future land use using a set of rules that spatially allocate population increases given among other factors, local land-use plans, existing city footprints, and existing/planned transportation routes (Johnston et al.,, 2003). Four-step travel demand models were obtained for all 8 counties within the SJV. As with most four-step models, factors that influence the amount and distribution of travel activities (e.g., household size, average income, auto ownership, and employment) are used to both replicate existing travel patterns and to forecast future patterns. Travel activity results are expressed in vehicle miles of travel (VMT) and vehicle speeds, which then serve as inputs for estimating mobile source emissions. UCDrive spatially and temporally allocates county-level emissions generated by MOBILE6 using link-based traffic activities generated from travel demand models (Niemeier et al., 2003). The spatial resolution of UCDrive is driven by a bicubic spline interpolation which increases the reliability of results when compared to a standard centroid, link approach (Niemeier and Zheng, 2004).

Biogenic emissions were generated for each 4 km × 4 km grid cell using the Biogenic Emission inventory Geographic Information System (BEIGIS) model developed by CARB. Hourly averaged temperature and surface shortwave radiation over the period of December 15th to January 7th were used as inputs to the model. Generation of the biogenic VOCs assumes a 2000 land-use pattern obtained from Moderate Resolution Imaging Spectroradiometer

Table 1
The general assumptions associated with each of the policy scenarios for 2030. Each row discusses 1) population density, 2) land-use assumptions and 3) emissions controls.

Scenario 1 "Population Growth"	Scenario 2 "Compact Growth"	Scenario 3 "Urban Sprawl"	Scenario 4 "Planned Growth"
Moderate population density and no land-use changes. Existing roadway network. No high-speed rail implementation.	Highest population density with tight land-use restrictions. Existing roadway network. High-speed rail implementation.	Sparse population density with unrestricted land use. 2030 roadway network. No high-speed rail implementation.	Moderate population density with planned land-use changes only. 2030 roadway network. High-speed rail implementation.
No new emission controls	Additional emissions controls	No new emissions controls	Only planned emissions controls

(MODIS) satellite data to determine leaf area index. The emissions of isoprene, monoterpenes and other volatile organic compounds (OVOCs) are calculated using equations found in (Guenther et al., 1993). MBO (2-methyl-3-buten-2-ol) was calculated using equations from (Harley et al., 1998).

3.2. Scenario development

The integrated emissions modeling system described above was applied to four unique scenarios to explore the effect of regional policies on air quality in the SJV. Each scenario assumes the same
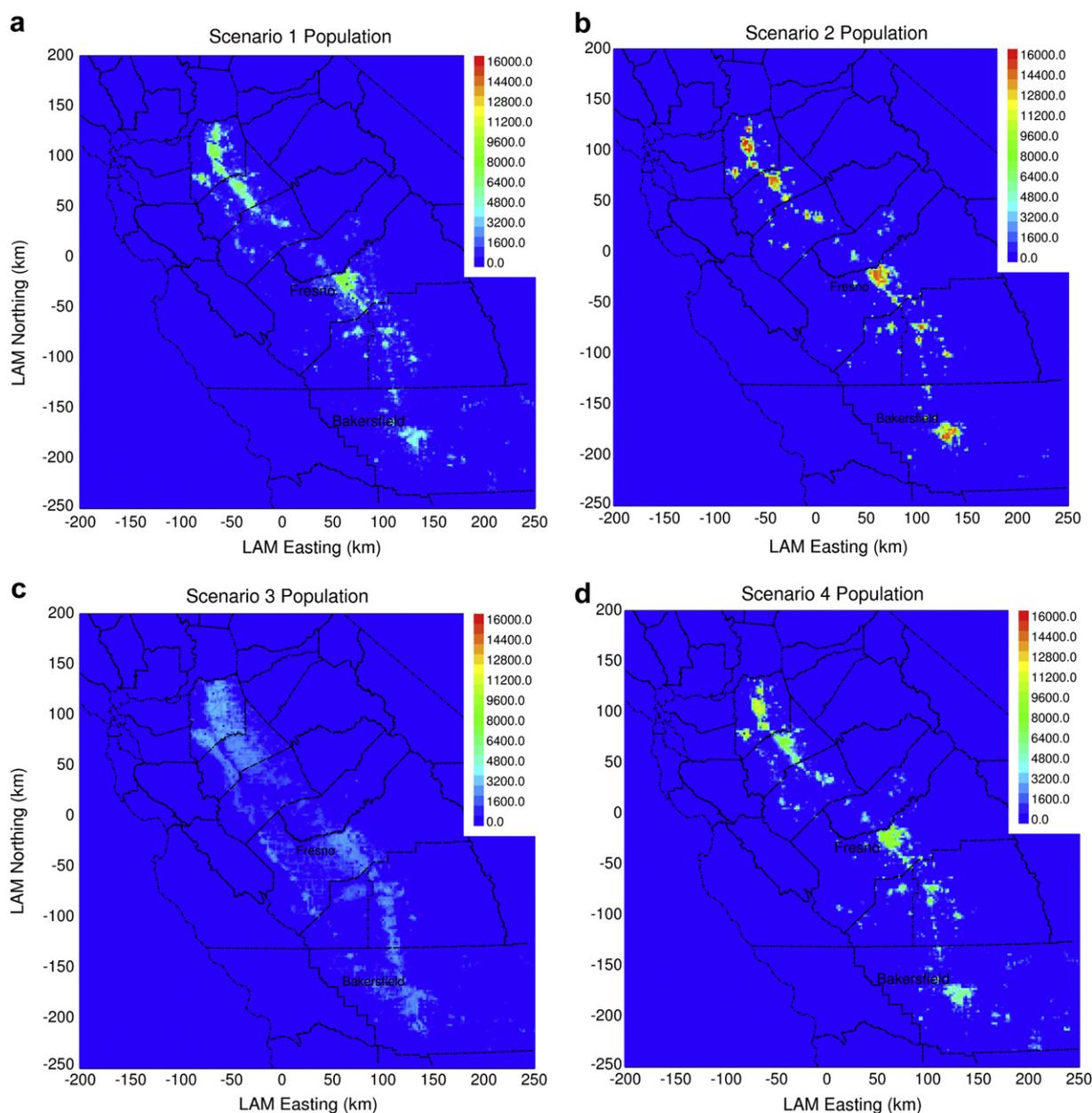
Fig. 1. Population in the San Joaquin Valley in the year 2030 under (a) static, (b) high density, (c) low density, and (d) as-planned regional policies. Values are given in raw population totals per 4 km² grid cell.

overall population increase of approximately +3 M people in the SJV by the year 2030 based on Department of Finance estimates (2004). The defining characteristics for each scenario are assumptions about land-use policies and transportation infrastructure investments although various other factors were also changed to explore the range of possible emissions outcomes.

Table 1 summarizes the major features of the four scenarios developed in the current study to demonstrate the sensitivity of air quality to policy boundaries. Scenario 1 reflects existing land-use patterns and transportation infrastructure but with population and employment growth. This scenario demonstrates the long-term outcomes from maintaining current patterns as population increases. Scenario 2 is a best-case scenario defined by compact urban footprints including redevelopment of existing urban centers to increase population density. This scenario includes infrastructure investments such as high-speed rail, and adoption of clean technology/policies that should lead to reduced emissions. Scenario 3 allows sprawling developments in the SJV and all planned investments in highways with little adoption of new technologies or other policies to reduce emissions. Finally, Scenario 4 reflects existing land use and transportation plans as well as other policies related to technology change that are likely to be adopted. All of the policy and technology changes
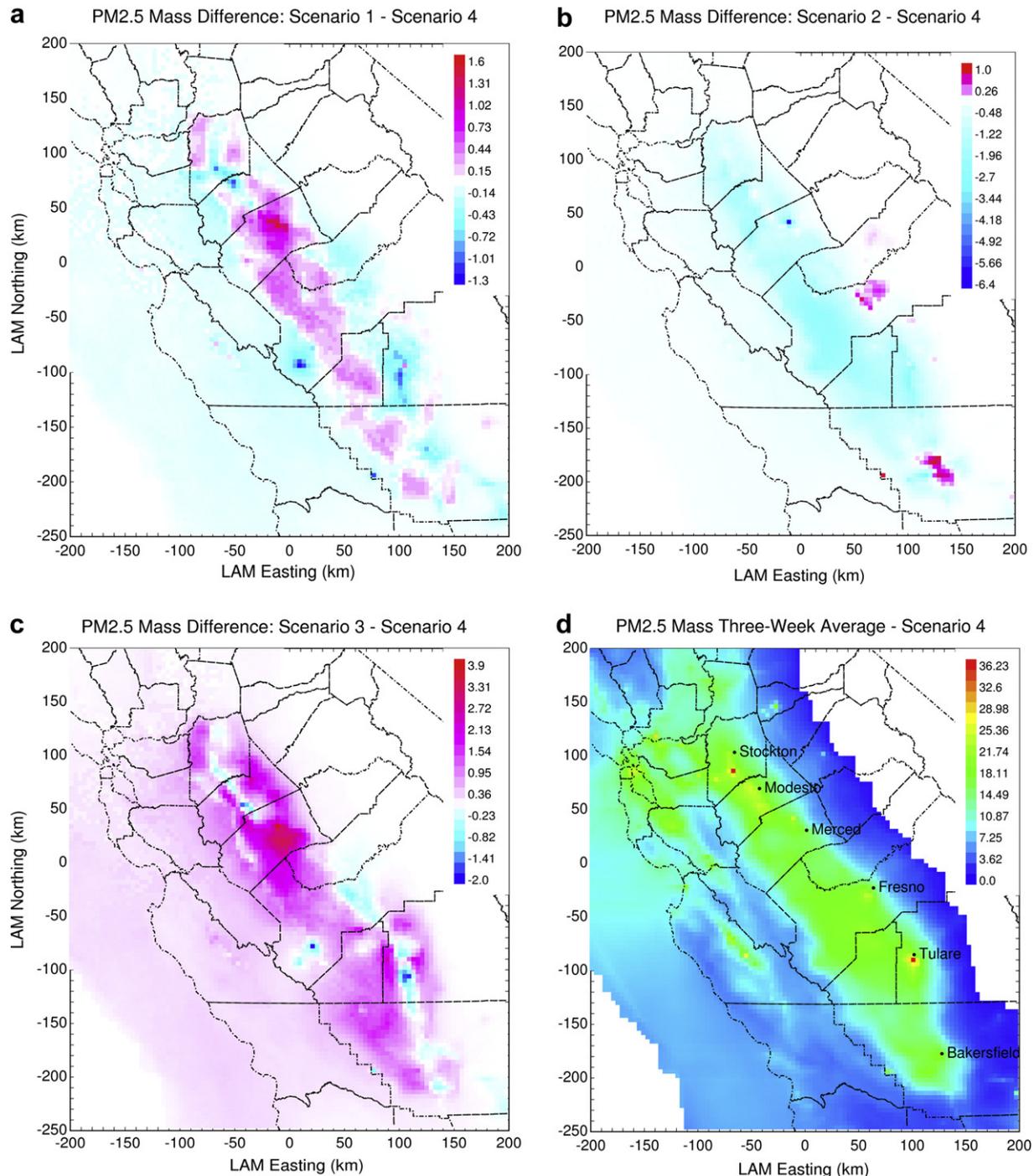
Fig. 2. PM2.5 mass concentrations in the year 2030 averaged over a 22-day air pollution event. Base-case concentrations (panel d) are shown as absolute values ($\mu g\ m^{-3}$). Concentrations in scenarios 1–3 (panels a–c) are shown as differences relative to the base-case ($\mu g\ m^{-3}$).

used to define the scenarios were developed with recommendations from an expert panel representing regulatory, transportation, agricultural, and business interests within the SJV.

Land-use policies and transportation infrastructure investments are focal points in the current study because they are key determinants of travel patterns, as established both theoretically and empirically (Hensher et al., 1993; Kenworthy and Laube, 1999; Handy, 2005). Land-use patterns and transportation networks resulting from policy decisions and infrastructure investments are key inputs into travel demand forecasting models that are used to estimate urban growth. It is therefore no surprise that the smart growth concept focuses on both land-use policies and infrastructure investments. Most of today's standard travel demand forecasting models are generally not capable of testing the more detail-oriented smart growth policies, such as street design standards. The counties included in the present study all use standard travel demand models and so we have focused on those policies that can be applied within these standard models to influence the location + density of population + employment and the capacity of highways.

The UPlan land-use model was used to predict the pattern of residential, industrial, commercial, and agricultural land use with 2 km spatial resolution over the entire SJV. Population and employment growth in each grid cell were projected using decision rules that reflected specific assumptions about land preservation and development strategies. For example, higher maximum population density limits were established in Scenario 2 to encourage controlled growth of urban boundaries. Population was increased inside existing cities, after which new growth occurred in adjacent grid cells with attractors such as existing transportation infrastructure.

Fig. 1 illustrates that population density varies greatly between scenarios 1–4. This figure displays the population in a given grid cell. Population densities are obtained by dividing the cell's population by the cell area, 4 km^2. The maximum population density of 3935 people km^{-2} occurs in Scenario 2 (Fig. 1b) in the city of Stockton. Similarly, most of the urban areas in Scenario 2 reflect an average density ≥3000 people km^{-2}. For reference, New York City has an average density of 2050 people km^{-2}, San Francisco has an average of 2350 people km^{-2}, Mexico City (Mexico) has an average of 8450 people km^{-2}, and Mumbai (India) has an average of 29,450 people km^{-2}. By contrast Scenario 3 (Fig. 1c) distributes population more uniformly throughout the SJV with a maximum density of 750 people km^{-2}. Scenarios 1 and 4 (Figs. 1a, and 2d) have maximum population densities of 2000 people km^{-2} and 2900 people km^{-2} respectively.

Population patterns and land use/land cover patterns are frequently used as surrogates to distribute area source emissions with greater spatial accuracy inside a coarsely defined region such as a county (Funk, 2001). In the present study, the population and employment distributions and land-use patterns predicted by UPlan were used to produce spatial allocations factors (SAFs) that converted county-level emissions from non-transportation sources to individual grid cells.

Table 2 summarizes the assumptions about technology and policy implementations that were added to each of the scenarios summarized in Table 1. Some of these additional policy changes were made uniformly across all scenarios because they are necessary to reduce future PM2.5 concentrations to levels close to the NAAQS. As one example, all scenarios assume a complete ban on residential wood combustion during the winter months. Other than this, Scenario 1 remains mostly static in terms of policy and infrastructure at the 2000 year emissions with the exception of population growth. Scenario 2 will see expansion in passenger rail, agricultural land preservation, decentralized power generation, application of diesel engine retrofitting, and alternative energy production. Agricultural dust emissions decrease by 50% in scenario 2. Scenario 3 expands freight and air transportation at Fresno by 50%. Scenario 3 also projects an increase in the states dairy cow population by 50% and a decrease in agricultural dust by 25%. Changes in scenario 4 attempt to best follow the current plans for freight and passenger rail expansion, planned air transport expansion at Fresno, agricultural land preservation trends, the current California Energy Commission power decentralization plans, a 25% reduction of agricultural dust and 20% increase in the dairy cow population. For all the scenarios, emissions outside the SJV were maintained at the base-case 2030 projections since the main goal of this study is to determine the impact of regional policies within the SJV.

Scenario 3 has the highest emissions of total organic gases (TOG), ROG, carbon monoxide (CO), NOx, oxides of sulfur (SOx), ammonia (NH$_3$), TSP, and particulate matter with aerodynamic diameter less than 10 μm and 2.5 μm (PM10 and PM2.5) while scenario 2 has the lowest emissions totals (see Table S1 in SI). Scenarios 1 and 4 lie in the middle, with scenario 4 showing slightly higher totals than scenario 1. Changes to transportation reduce NOx emissions in scenario 2. This reduction is partly from reduced VMT for on-road mobile sources and partly from trains and off-road sources. ROG emissions decline due to changes in farming operations in scenario 2. Likewise farming operations account for the bulk of the PM2.5 emissions reductions as well. NOx increases in scenario 3 are largely explained by the higher VMT resulting from urban sprawl. ROG emissions are driven upwards in scenario 3 as a result of farming operations. PM2.5 emitted from farming operations also drives up the totals in scenario 3.

3.3. Air quality modeling

The impact of the emissions from scenarios 1–4 on air quality was evaluated using the meteorological data that was collected during the California Regional Particulate Air Quality Study (CRPAQS). The meteorological observations were used to generate a set of diagnostic meteorological data as described by Ying et al. (2008). Meteorology was selected during a three week stagnation episode between

Table 2
The additional technology and control assumptions associated with each of the policy scenarios for 2030. Each control represents a policy choice that does not fit in the general categories of Table 1.

Variable	Scenario 1	Scenario 2	Scenario 3	Scenario 4
Transportation Rail	No Expansion	Passenger Expansion	Freight Expansion	Freight and Passenger Expansion
Transportation Air	No Expansion	No Expansion	Expand as Planned at Fresno	Expand as Planned at Fresno
Ag Land Preservation	Maintain acres with no increase	Large acreage increase	Maintain acres with no increase	Follow acreage changes trends
Decentralized Power Generation	No Decentralized Power	Upper Bound of Power Generation	No Decentralized Power	Implement CEC plan
Reduced Wood Combustion	Complete ban	Complete ban	Complete ban	Complete ban
Agricultural Emissions – Diesel	No change	Retrofit engines	No change	No change
Agricultural Emissions – Dust	No change	50% reduction	25% reduction	25% reduction
Agricultural Emissions – Dairy	No change	No change	50% increase in cow population	20% increase in cow population
Alternative energies	No change	38% increase	No change	No change
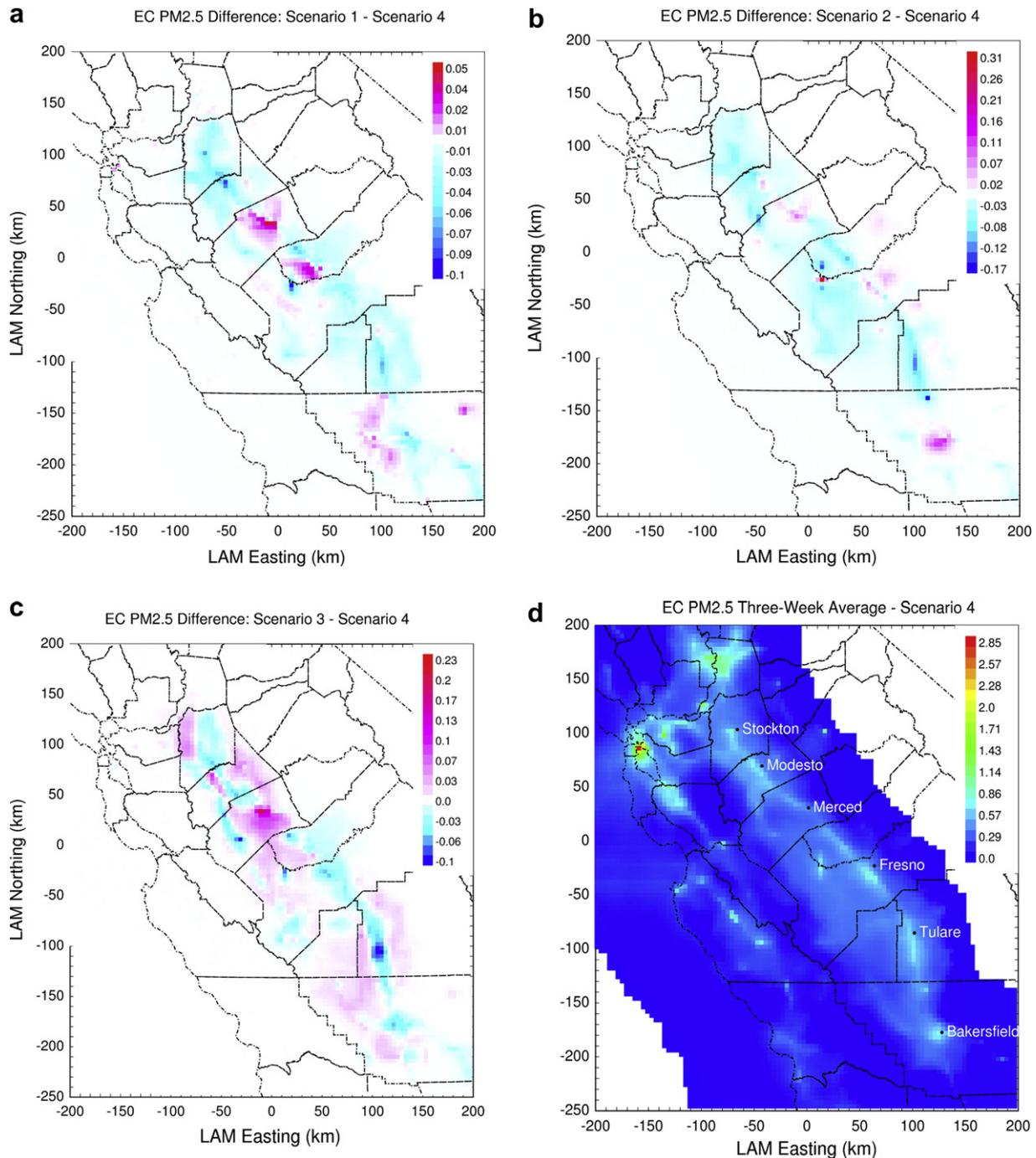
Fig. 3. PM2.5 EC concentrations in the year 2030 averaged over a 22-day air pollution event. Base-case concentrations (panel d) are shown as absolute values ($\mu g\ m^{-3}$). Concentrations in scenarios 1–3 (panels a–c) are shown as differences relative to the base-case ($\mu g\ m^{-3}$).

December 15, 2000 and January 7, 2001. Initial conditions and boundary conditions for the simulation were also set at values measured during CRPAQS. Previous studies have shown that initial conditions are generally washed out of the simulation after approximately 2–3 days, with the remaining air quality determined by the balance between emissions and meteorology.

The species listed in the raw emissions inventory were converted to inputs for air quality modeling through the use of source profiles that describe the composition of NMOG and TSP. Hourly emissions data for each day of the model period was assigned to 4 km by 4 km cells on a 190 by 190 Lambert Conformal grid covering all of Central

California. Emissions were split into separate files based on eight broad source categories: gasoline engines, diesel engines, wood smoke, food cooking, natural gas combustion, high-sulfur fuel combustion, crustal material including road dust, and other primary sources. These source-oriented emissions inventories were fed into the UCD source-oriented three dimensional photochemical air quality grid model (Kleeman and Cass, 2001; Ying et al., 2008; Ying and Kleeman, 2009). The UCD air quality model was configured with seven vertical layers that varied in thickness from 35 m at the surface up to 500 m at the top of the domain (5 km). A modified version of the SAPRC90 chemical mechanism (Ying et al., 2007) was used to predict
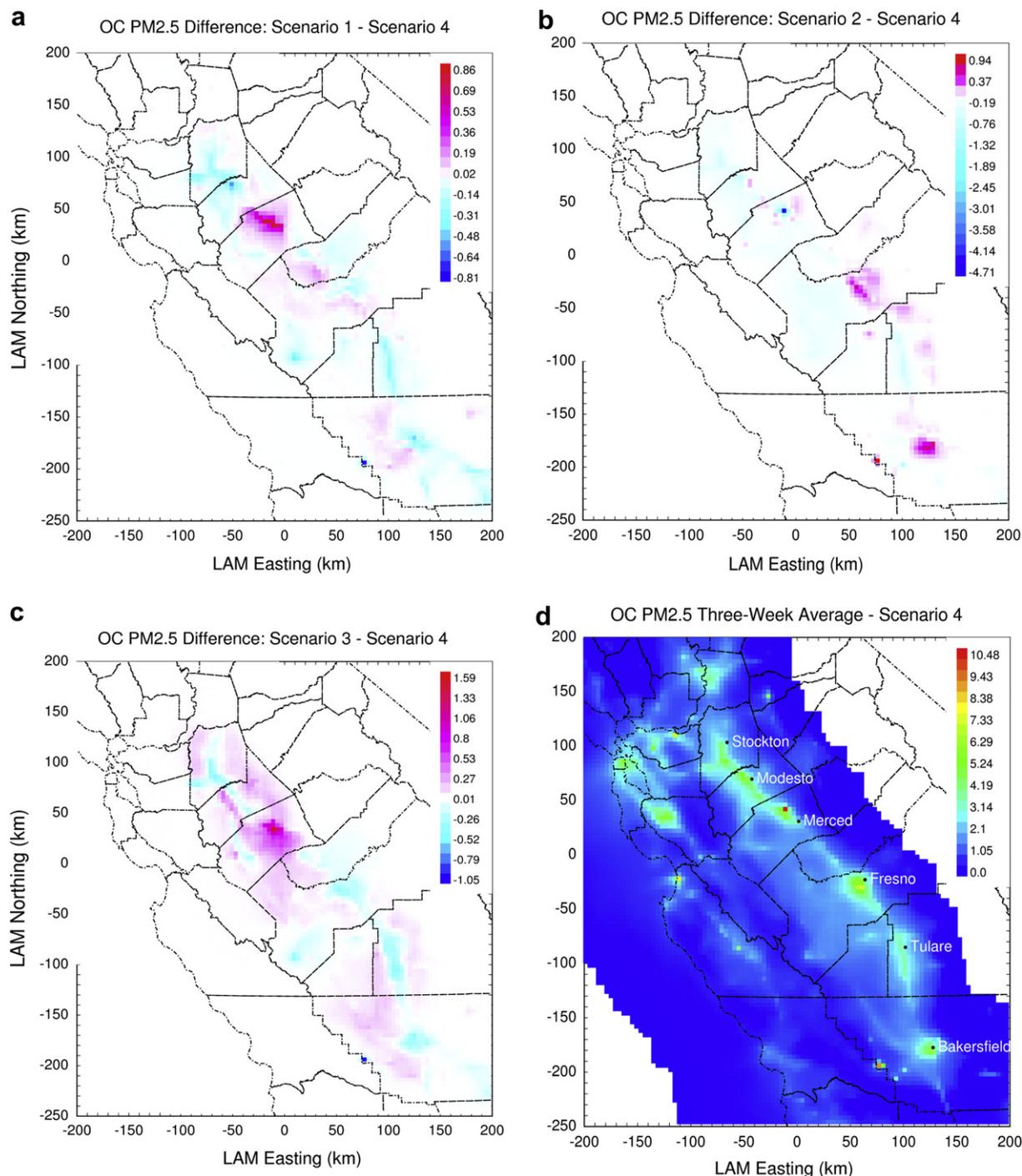
Fig. 4. PM2.5 OC concentrations in the year 2030 averaged over a 22-day air pollution event. Base-case concentrations (panel d) are shown as absolute values ($\mu g\ m^{-3}$). Concentrations in scenarios 1–3 (panels a–c) are shown as differences relative to the base-case ($\mu g\ m^{-3}$).

gas-phase reactions. Airborne particulate matter was represented using 15 size bins evenly spaced on a logarithmic scale between 0.01 and 10.0 μm. Gas-particle conversion reactions were represented using the solution to the dynamic equations developed by Jacobson (2005). Equilibrium vapor pressures for nitric acid, hydrochloric acid, and ammonia were calculated using the thermodynamic model ISORROPIA II (http://nenes.eas.gatech.edu/ISORROPIA) (Nenes et al., 1998; Fountoukis and Nenes, 2007). Secondary organic aerosol formation was predicted using an absorption model based on data obtained from smog chamber studies (Ying et al., 2007).

Simulations for each scenario described in Section 3.2 were completed at both 4 km and 8 km horizontal resolution. Coarser spatial resolution greatly increased the speed of the simulation with little loss of accuracy under the meteorological conditions used in the present study (Ying et al., 2008).

4. Results

PM2.5 concentration predictions in the SJV were averaged over the 22-day period December 17th through January 7th. The first two
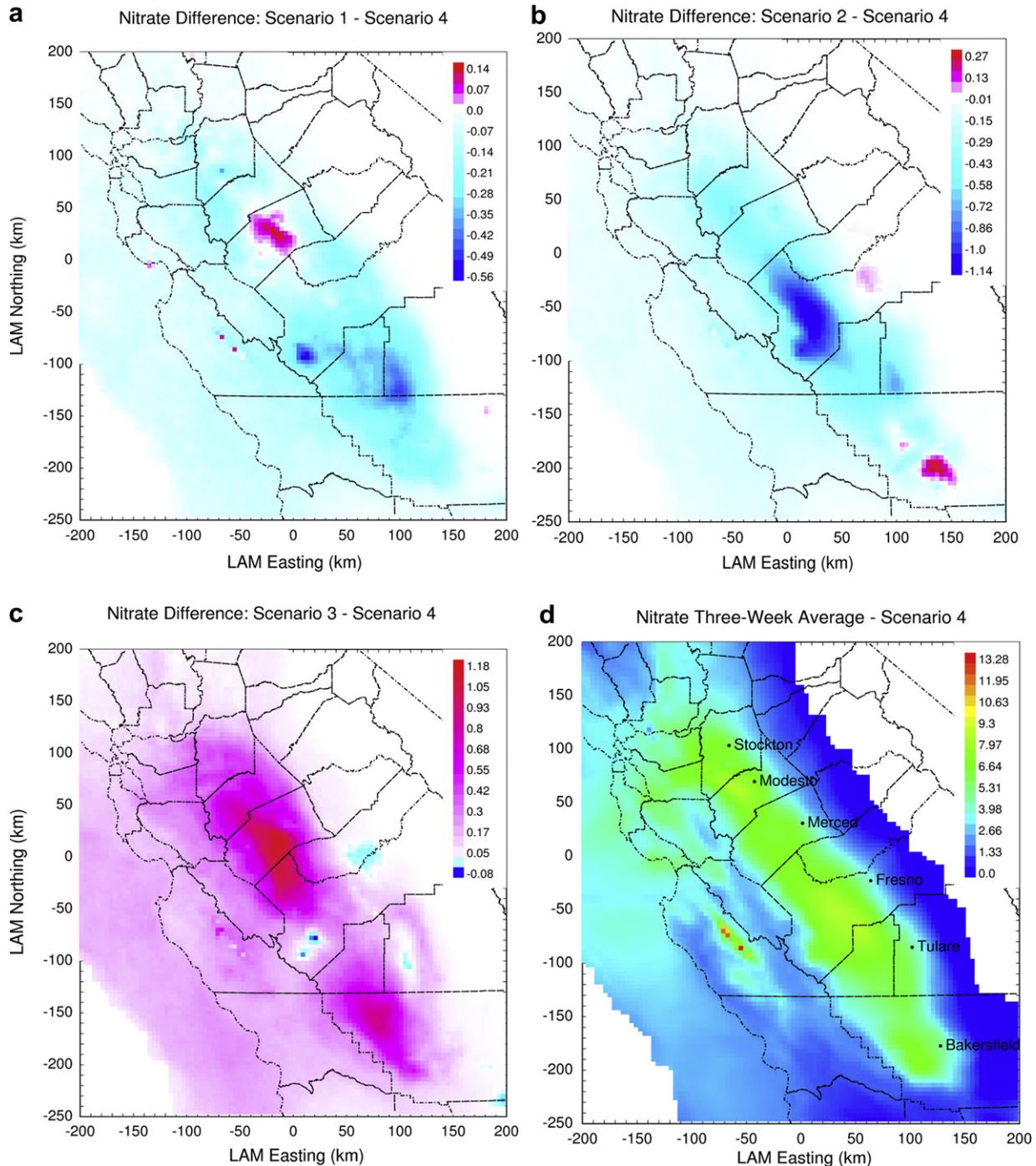
Fig. 5. PM2.5 nitrate concentrations in the year 2030 averaged over a 22-day air pollution event. Base-case concentrations (panel d) are shown as absolute values ($\mu g\ m^{-3}$). Concentrations in scenarios 1–3 (panels a–c) are shown as differences relative to the base-case ($\mu g\ m^{-3}$).

days of each simulation were not included in the results in order to minimize the effects of initial conditions. Base-case (scenario 4) concentrations are presented along with the changes induced by scenarios 1–3 relative to the base-case. Results are displayed for PM2.5 mass as well as the major components that contribute to that mass including EC, OC, and nitrate. It is important to reiterate that model results are not forecasts, but rather a comparison between four possible scenarios that share common factors but differ on several important policy assumptions. The variation between scenarios quantifies the effects of those policies with all other factors held constant.

Figs. 2 through 5 show the average hourly results over 22 days for PM2.5 total mass, EC, OC and nitrate for the four scenarios. The base-case results for scenario 4 are presented in the bottom right of each panel (Figs. 2d, 3d, 4d, and 5d). Scenarios 1–3 are shown as difference plots relative to this base-case.

Scenario 4's predicted base-case PM2.5 mass concentrations averaged over 22 days exceed the 24-h average PM2.5 NAAQS of $35\ \mu g\ m^{-3}$ near Stockton, CA and Tulare, CA (Fig. 2d). Much of the SJV has ambient concentrations around $25\ \mu g\ m^{-3}$. Fig. 3d presents base-case elemental carbon concentrations for the 22-day period. Base-case concentrations are highest along Highway 99 and in

Fig. 6. Population-weighted PM2.5 concentrations in the year 2030. Panel (a) shows the concentrations experienced by the average resident in the SJV. Panel (b) shows the concentrations experienced by the 10% of residents in the SJV with the highest exposure.

in a single grid cell. More typically, decreases in scenario 2 PM2.5 concentrations of 1 μg m^{-3} are observed over the majority of the rural areas in the SJV. Scenario 2 PM2.5 concentrations in urban areas are predicted to increase by 1.0 μg m^{-3} relative to the base-case. The greatest changes for EC relative to the base-case are observed in scenario 2 (Fig. 3b). The largest increase of 0.3 μg m^{-3} and the largest decrease of 0.2 μg m^{-3} both occur in single grid cells. More typical behavior is described by urban increases of 0.2 μg m^{-3} and rural sites decreases of 0.1 μg m^{-3}. Scenario 2 (Fig. 4b) exhibits the greatest reduction in predicted OC concentrations with a decrease of 4.7 μg m^{-3} relative to base-case concentrations. More typically, most rural sites experienced a <1 μg m^{-3} decrease in OC concentrations relative to the base-case while OC concentrations in urban centers increased by 0.5 μg m^{-3}. Scenario 2 nitrate concentrations in Fresno County exhibit the largest decline of 1.1 μg m^{-3} relative to base-case concentrations (Fig. 5b). For most of the region, decreases in nitrate are on the order of 0.5 μg m^{-3} in scenario 2, with a slight increase of 0.3 μg m^{-3} in Bakersfield.

Increased concentrations are highest for scenario 3, with concentrations 3.9 μg m^{-3} above base-case values around Merced County and 1–2 μg m^{-3} above base-case values in rural areas. Scenario 3 PM2.5 concentrations in urban areas are 0.5–2.0 μg m^{-3} lower than base-case values. Scenario 3 (Fig. 3c) exhibits the opposite trend compared to scenario 2. Scenario 3 EC concentrations are 0.1 μg m^{-3} higher in rural areas and 0.05 μg m^{-3} lower in urban areas. Scenario 3 (Fig. 4c) has the largest increases of 1.6 μg m^{-3} over the base-case in rural areas of Merced County. Urban sites in scenario 3 experience a ~0.3 μg m^{-3} decrease in OC concentrations. Maximum increases of up to 1.2 μg m^{-3} relative to base-case concentrations are seen in rural areas for Scenario 3 (Fig. 5c). Regional nitrate concentrations generally increase between 0.5 and 1.0 μg m^{-3} in scenario 3. Trends for ammonium ion and sulfate are illustrated in SI Figures S2 and S3.

The population distributions shown in Fig. 1 can be combined with the particulate matter trends illustrated in Figs. 2–5 in order to fully evaluate human PM2.5 exposure. Fig. 6 compares the population-weighted average PM2.5 mass exposure between the four scenarios considered in the present study. The results are organized to show the average population exposure using all residents in the SJV (Fig. 6a) and the 10th percentile of residents who experience the highest PM2.5 exposure during the current study (Fig. 6b). Results under each scenario are broken down by chemical component contribution to the particulate matter mass. Fig. 6a illustrates that all of the scenarios have very similar population-weighted average PM2.5 exposure. The maximum population-weighted average PM2.5 exposure of 17.4 μg m^{-3} occurs in scenario 2. The lowest population-weighted average PM2.5 exposure of 16.0 μg m^{-3} occurs in scenario 1. Fig. 6b illustrates that the maximum 10th percentile exposure of 25.4 μg m^{-3} occurs is in scenario 4, while the lowest 10th percentile exposure of 24.6 μg m^{-3} occurs in scenario 3.

Fig. 7 illustrates the percent change in population-weighted average exposure to PM2.5 chemical components for scenarios 1–3 relative to the base-case (scenario 4). Results are shown for the total population-weighted average (Fig. 7a) and the top 10th percentile population-weighted average (Fig. 7c). Fig. 7a demonstrates that the PM2.5 component exposure differs significantly between the various scenarios. Average EC and OC exposure increases by 10% and 15% respectively in scenario 2 compared to the base-case. Ammonium, sulfate and nitrate values increase by less than 5% in scenario 2. In contrast, scenario 3 EC and OC exposure is 11% and 19% lower than the base-case, respectively. Scenario 3 nitrate and ammonium ion exposure is 10% higher than the base-case, while sulfate exposure is 5% lower. The trends illustrated in Fig. 7c for the top 10th percentile of PM2.5 exposure are similar to those in Fig. 7a for total population exposure. Fig. 7c shows that EC and OC exposure is increased by 7% and 11% respectively in scenario 2 over the

urban areas with peak values under 0.9 μg m^{-3}. The spatial concentration pattern of OC is similar to EC (Fig. 3d) with higher values around urban centers and along the transportation corridors (Fig. 4d). Base-case values peak at 10 μg m^{-3} with most urban centers reaching 6 μg m^{-3}. Concentrations quickly fall below 2 μg m^{-3} outside of urban centers. Base-case nitrate concentrations seen in Fig. 5d are smoother than EC and OC gradients because nitrate is a secondary pollutant produced by regional atmospheric chemistry. Nitrate concentrations vary from <3 μg m^{-3} along the edge of the SJV to >9.5 μg m^{-3} in the center of the SJV. The maximum value of 13 μg m^{-3} occurs west of the SJV region.

Scenario 1 exhibits a PM2.5 increase of 1.6 μg m^{-3} relative to the base-case in Merced County, with mixed regions of increase/decrease over the remainder of the SJV (Fig. 2a). Scenario 1 EC increases a maximum of 0.05 μg m^{-3} along transportation corridors and near Merced (Fig. 3a). Scenario 1 decreased up to 0.1 μg m^{-3} at rural sites. Fig. 4a shows OC increases by 0.9 μg m^{-3} in large areas around Merced, and decreases by 0.8 μg m^{-3} at a single grid cell the western edge of the SJV. For the most part, scenario 1 OC concentrations fluctuate by ±0.2 μg m^{-3} throughout the SJV. Scenario 1 nitrate (Fig. 5a) exhibits a mixture of increasing and decreasing concentrations, with an overall regional decrease of 0.2 μg m^{-3}.

Compact growth produces the largest decline in PM2.5 mass of 6.4 μg m^{-3} relative to base-case values but this decrease is localized

Fig. 7. Percent change in population-weighted exposure to PM2.5 concentrations (panels a and c) or emissions (panels b and d) relative to base-case (scenario 4). Panels (a and c) show the change experienced by the average resident in the SJV. Panel (c) shows the change experienced by the 10% of residents in the SJV with the highest exposure.

base-case. Nitrate, sulfate and ammonium ion exposure decrease by less than 5% in scenario 2 relative to the base-case. EC and OC exposure in the top 10th percentile of the population declines in scenario 3 by 16% and 22%. Nitrate exposure in the top 10th percentile of the population is 12.5% over the base-case, while ammonium ion exposure increases by 7.7%. Sulfate exposure decreases from base-case values by 13% in scenario 3.

5. Discussion

Although population-weighted exposure to total PM2.5 is similar for all the scenarios (Fig. 6), the population exposure to different particulate matter chemical components tells a more complex story (Fig. 7a and c). While the compact growth coupled with clean technology adoption represented in scenario 2 leads to a region-wide reduction in PM2.5 concentrations, the localization of primary PM around dense population centers leads to higher population-weighted exposure for EC and OC. Exposure to nitrate, sulfate and ammonium is lower across the region for scenario 2 compared to the as-planned base-case (scenario 4). The population-weighted exposure to PM components observed in scenario 3 (low-density development, without clean technology adoption) are opposite those observed for scenario 2 (compact). PM2.5 EC and OC are still largely localized around major transportation corridors and urban centers but the low-density population pattern moves people away from these high concentration regions. Regional PM2.5 nitrate and ammonium ion concentrations are significantly higher in the low-density scenario, resulting in higher population exposure for these pollutants relative to base-case concentrations.

Recent epidemiological studies have found significant correlations between adverse human health effects and exposure to primary PM components such as EC, with less significant findings for secondary components such as nitrate (Ostro et al., 2007). The trends identified in the current study suggest that there may be some density threshold at which the benefits of higher density begin to be outweighed by the disbenefits of increased air pollution. Using this population-weighted exposure approach, thresholds could be

defined to ensure that long-term urban growth produce optimal air quality benefits.

Significant expertise in air quality modeling is required to produce the results in Figs. 2–5. This level of analysis is often beyond regional agencies when they are preparing urban growth plans. It may be possible to identify the most important conclusions about population-weighted exposure to primary pollutants and the best locations for future urban growth using a simplified direct analysis of population-weighted average emissions. Fig. 7b and d illustrates the percent change in population-weighted average emissions relative to the base-case conditions in the present study. Fig. 7b shows results for the entire population, while Fig. 7d shows results for the 10th percentile of the population that experiences the maximum PM2.5 exposure. Comparing Fig. 7a with c one sees the trends in population-weighted exposure to EC and OC tracks with the trends in population-weighted emissions. Increasing the population-weighted emissions leads to increases in exposure to primary components. Decreasing the population-weighted emissions decreases the population-weighted exposure. The trends in the percentage difference in the weighted emissions are approximately double the trends in the weighted PM2.5 concentrations. A 30% increase in weighted OC emissions in scenario 2 translates to 15% increase in OC exposure. Similarly, the weighted emissions of OC are 40% lower in scenario 3 while the OC exposure values are 20% lower than the base-case. Population-weighted emissions does not usurp analysis using the photochemical transport model because exposure to secondary particulate matter (i.e. nitrate and ammonium ion) and total PM mass can only be evaluated using the more rigorous modeling technique. Nonetheless, the simplified inventory analysis could be carried out by regional agencies as a preliminary calculation to help guide future decisions about urban land-use development.

6. Conclusion

Four scenarios for air pollution emissions in the year 2030 were developed for California's San Joaquin Valley. Each scenario was

evaluated during an air pollution episode using the meteorology observed between December 15, 2000 and January 7, 2001. Close examination of the population exposure to different PM2.5 chemical components under each scenario reveals two different trends for scenarios involving high population density and low population density. The more compact development scenario leads to increased exposure to primary PM2.5 such as EC and OC caused largely by increased population density around major transportation corridors and other pre-existing urban sources. Reductions in vehicle miles traveled and controls on other combustion sources inherent in the compact development scenario caused an overall decrease in regional NOx emissions resulting in decreased exposure to nitrate and ammonium ion. This decrease in exposure to secondary pollutants is not directly related to the shifting population footprint since secondary pollutants are more evenly distributed throughout the region.

The low population density scenario increased regional PM2.5 concentrations but produced lower overall population-weighted exposure to primary PM2.5 components such as EC and OC. The low-density scenario moved residents of the SJV away from the largest sources of primary PM2.5 including the major transportation corridors. The low-density development scenario caused increased exposure to PM2.5 nitrate and ammonium ion because NOx emissions increased due to the need for increased driving distances and the adoption of less rigorous emissions controls.

Compact, high density urban development combined with rigorous pollution control measures at the local level can significantly reduce regional PM concentrations. In the San Joaquin Valley of California, the difference between a low-density urban growth plan vs. a high density urban growth plan amounts to a 20% shift in regional PM2.5 concentrations. The benefits of high density urban growth for population-weighted exposure are not as obvious. Future development plans should consider population-weighted average exposure to primary pollutant emissions as a simple metric to decide appropriate locations for growth.

Acknowledgments

Appendix. Supplementary information

Supplementary data associated with this article can be found in the online version at doi:10.1016/j.atmosenv.2009.10.041.

References

Brownstone, D., Golob, T.F., 2009. The impact of residential density on vehicle usage and energy consumption. Journal of Urban Economics 65, 91–98.

California Department of Finance, 2004. Population Projections by Race/Ethnicity for California and Its Counties, 2000–2050. California Department of Finance, Sacramento, California.

Englert, N., 2004. Fine particles and human health – a review of epidemiological studies. Toxicology Letters 149, 235–242.

Fountoukis, C., Nenes, A., 2007. ISORROPIA II: a computationally efficient thermo-dynamic equilibrium model for $K^+-Ca^{2+}-Mg^{2+}-NH_4^+-Na^+-SO_4^{2-}-NO_3^--Cl^--H_2O$ aerosols. Atmospheric Chemistry and Physics 7, 4639–4659.

Funk, T.H., 2001. Development of Gridded Spatial Allocation Factors for the State of California. Sonoma Technology, Inc., Petaluma, CA.

Guenther, A.B., Zimmerman, P.R., Harley, P.C., Monson, R.K., Fall, R., 1993. Isoprene and monoterpene emission rate variability – model evaluations and sensitivity analyses. Journal of Geophysical Research Atmosphere 98, 12609–12617.

Handy, S., 2005. Smart growth and the transportation – land use connection: what does the research tell us? International Regional Science Review 28, 146–167.

Harley, P., Fridd-Stroud, V., Greenberg, J., Guenther, A., Vasconcellos, P., 1998. Emission of 2-methyl-3-buten-2-ol by Pines: a Potentially Large Natural Source of Reactive Carbon to the Atmosphere. American Geophysical Union.

Hensher, D.A.I., Salomon, P., BovyOrfeuil, J.-P., 1993. A Billion Trips Per Day: Tradition and Transition in European Travel Patterns. Kluwer Academic Publishers Group, Dordrecht, The Netherlands.

Herner, J.D., Aw, J., Gao, O., Chang, D.P.Y., Kleeman, M.J., 2005. Size and composition distribution of airborne particulate matter in Northern California. 1. Particulate mass, carbon, and water soluble ions. Journal of the Air & Waste Management Association, 55, 30–51.

Jacobson, M.Z., 2005. A solution to the problem of nonequilibrium acid/bas gas-particle transfer at long time step. Aerosol Science and Technology 39, 92–103.

Johnston, R.A., Shabazian, D.R., Gao, S., 2003. UPlan: a versatile urban growth model for transportation planning. Transportation Research Record 1831, 202–209.

Kahyaoglu-Koracin, J., Bassett, S.D., Mouat, D.A., Gertler, A.W., 2009. Application of a scenario-based modeling system to evaluate the air quality impacts of future growth. Atmospheric Environment 43, 1021–1028.

Kenworthy, J.R., Laube, F.B., 1999. Patterns of automobile dependence in cities: an international overview of key physical and economic dimensions with some implications for urban policy. Transportation Research Part A: Policy and Practice 33, 691–723.

Kleeman, M.J., Cass, G.R., 2001. A 3D Eulerian source-oriented model for an externally mixed aerosol. Environmental Science and Technology 35, 4834–4848.

Krizek, K.J., 2003. Residential relocation and changes in urban travel – Does neighborhood-scale urban form matter? Journal of American Planning Association 69, 265–281.

Magliano, K.L., Hughes, V.M., Chinkin, L.R., Coe, D.L., Haste, T.L., Kumar, N., Lurmann, F.W., 1999. Spatial and temporal variations in PM10 and PM2.5 source contributions and comparison to emissions during the 1995 integrated monitoring study. Atmospheric Environment 33, 4757–4773.

Nenes, A., Pandis, S.N., Pilinis, C., 1998. ISORROPIA: a new thermodynamic equilibrium model for multiphase multicomponent inorganic aerosols. Aquatic Geochemistry 4.

Niemeier, D., Zheng, Y., Kear, T., 2003. UCDrive: a new gridded mobile source emissions inventory model. Atmospheric Environment 38, 305–319.

Niemeier, D.A., Zheng, Y., 2004. Impact of finer grid resolution on the spatial distribution of vehicle emissions inventories. Environmental Science and Technology 38, 2133–2141.

Ostro, B., Feng, W.Y., Broadwin, R., Green, S., Lipsett, M., 2007. The effects of components of fine particulate air pollution on mortality in California: results from CALFINE. Environmental Health Perspectives 115, 13–19.

Puri, A., Kleinhenz, R.A., 1994. A Study to Develop Projected Activity for Non-road Mobile Categories in California, 1970–2020. California State University at Fullerton, Fullerton, California.

Stone, B., Mednick, A.C., Holloway, T., Spak, S.N., 2007. Is compact growth good for air quality? Journal of American Planning Association 73, 404–418.

Ying, Q., Fraser, M.P., Griffin, R.J., Chen, J.J., Kleeman, M.J., 2007. Verification of a source-oriented externally mixed air quality model during a severe photochemical smog episode. Atmospheric Environment 41, 1521–1538.

Ying, Q., Lu, J., Allen, P., Livingstone, P., Kaduwela, A., Kleeman, M., 2008. Modeling air quality during the California Regional PM10/PM2.5 Air Quality Study (CRPAQS) using the UCD/CIT source-oriented air quality model – Part I. Base case model results. Atmospheric Environment 42, 8954–8966.

Ying, Q., Kleeman, M., 2009. Regional contributions to airborne particulate matter in central California during a severe pollution episode. Atmospheric Environment 43, 1218–1228.